Title

Quinolinyl-based multitarget-directed ligands with soluble epoxide hydrolase and fatty acid amide hydrolase inhibitory activities: Synthetic studies and pharmacological evaluations

Journal

Heliyon, 10(11)

ISSN

2405-7843

Authors

Angelia, Jeannes

Duong, Leah

Yun, Faye

et al.

Publication Date

2024-06-01

DOI

10.1016/j.heliyon.2024.e32262

Peer reviewed

Heliyon 10 (2024) e32262

Contents lists available at ScienceDirect

Heliyon

journal homepage: www.cell.com/heliyon

Research article

Quinolinyl-based multitarget-directed ligands with soluble epoxide hydrolase and fatty acid amide hydrolase inhibitory activities: Synthetic studies and pharmacological evaluations

Jeannes Angelia [a], Leah Duong [a], Faye Yun [a], Anesa Mesic [a], Cassandra Yuan [b], Daniel Carr [b], Siena Gunari [b], Paula K. Hudson [a], Christophe Morisseau [c], Bruce D. Hammock [c], Ram Kandasamy [b,**], Stevan Pecic [a,*]

[a] Department of Chemistry & Biochemistry, California State University, Fullerton, 800 N. State College, Fullerton, CA, 92834, United States
[b] Department of Psychology, California State University, East Bay, 25800 Carlos Bee Blvd. Science S229, Hayward, CA, 94542, United States
[c] Department of Entomology and Nematology, and UCD Comprehensive Cancer Center, University of California Davis, Davis, CA, 95616, United States

ARTICLE INFO

Keywords:
Structure-activity relationship study
Enzyme inhibition
Multi-target directed ligands
Microwave-assisted synthesis
Suzuki coupling reaction
Molecular modeling
Formalin test

ABSTRACT

Simultaneous inhibition of soluble epoxide hydrolase (sEH) and fatty acid amide hydrolase (FAAH) with a single small molecule represents a novel therapeutic approach in treating inflammatory pain, since both targets are involved in pain and inflammation processes. In this study using multi-target directed ligands methodology we designed and synthesized 7 quinolinyl-based dual sEH/FAAH inhibitors, using an optimized microwave-assisted Suzuki-Miyaura coupling reaction and tested their potency in human FAAH and human, rat, and mouse sEH inhibition assays. The structure-activity relationship study showed that quinolinyl moiety is well tolerated in the active sites of both enzymes, yielding several very potent dual sEH/FAAH inhibitors with the IC_{50} values in the low nanomolar range. The most potent dual inhibitor **4d** was further evaluated in stability assay in human and rat plasma where it performed better than the standard Warfarin while *in vivo* study revealed that 1 mg/kg **4d** can inhibit acute inflammatory pain in male rats to a similar degree as the traditional nonsteroidal anti-inflammatory drug ketoprofen (30 mg/kg) after intraperitoneal injection. ADMET prediction studies for this dual inhibitor show favorable pharmacokinetic properties which will guide the future *in vivo* evaluations.

1. Introduction

Eicosanoids, encompassing prostaglandins, thromboxanes, leukotrienes, and epoxy fatty acids (EpFAs), are integral to a myriad of physiological processes, including inflammation, platelet aggregation, vasodilation, and nociception [1,2]. The endocannabinoid system (ECS) is a complex cell signaling system that regulates the central nervous system and plays an important role in synaptic communications and biological functions. Since the ECS impacts multiple biological and cellular functions, it is considered a potential therapeutic target for treatment of conditions and diseases such as pain, blood pressure, Alzheimer's disease, epilepsy, and anxiety

* Corresponding author.
** Corresponding author.
E-mail addresses: ram.kandasamy@csueastbay.edu (R. Kandasamy), specic@fullerton.edu (S. Pecic).

https://doi.org/10.1016/j.heliyon.2024.e32262
Received 12 February 2024; Received in revised form 16 May 2024; Accepted 30 May 2024
Available online 1 June 2024

[3–5].

The enzymatic roles of soluble epoxide hydrolase (sEH) and fatty acid amide hydrolase (FAAH) in both eicosanoid metabolism and the ECS are of significant relevance. The sEH mediates the hydrolysis of epoxyeicosatrienoic acids (EETs) and other epoxyfatty acids (EpFA), which are synthesized via the cytochrome P450 pathway from arachidonic acid (Fig. 1), converting them into their far more polar and sometimes pro-inflammatory counterparts. For the EET example these are dihydroxy-eicosatrienoic acids (DHETs) [6,7]. EETs are versatile in their physiological functions, with prominent vasodilatory, anti-inflammatory, and analgesic properties [8,9]. The absolute amounts of DHETs and EETs or the ratio of DHETs relative to EETs can be seen as a marker for reduced anti-inflammatory and analgesic actions in the system. Therefore, the equilibrium between EETs and DHETs, primarily controlled by sEH, is one important determinant of the inflammatory response and pain sensation [10,11]. Another hydrolytic enzyme, the amidase FAAH, hydrolyzes endocannabinoids, which are naturally produced molecules in the human body that are able to activate the cannabinoid receptors by binding to their active sites [5,12]. While the most studied endocannabinoids, anandamide (AEA) and 2-arachidonoyl glycerol (2-AG) are synthesized and metabolized differently, the degradation of these two endocannabinoids leads to the formation of arachidonic acid, a crucial precursor for inflammatory eicosanoids, and an inactive metabolite that cannot bind to cannabinoid receptors and produce potential therapeutic effects (Fig. 1) [13]. Given the profound implications of these enzymes in modulating pain and inflammation, both sEH and FAAH have emerged as central targets in therapeutic research [14–19].

The combined inhibition of sEH and FAAH presents a logical approach to pain management, drawing from the known functions of these enzymes in pain and inflammatory pathways. Sasso et al. (2015), showed that a synergistic reduction in both inflammatory and neuropathic pain was observed in rodent models when these two enzymes were simultaneously inhibited by FAAH inhibitor URB937 and sEH inhibitor TPPU [20]. This observed synergy further bolsters the proposition that a dual sEH/FAAH inhibition strategy can maximize therapeutic pain relief while likely minimizing adverse effects.

For the past several years, our group has been working on developing dual sEH/FAAH inhibitors [21–24] using the multi-target directed ligands (MTDLs) approach, a medicinal chemistry method where a single drug modulates two or more biological targets simultaneously [25]. Here, we report the structure-activity relationship (SAR) study coupled with docking experiments of quinolinyl-phenyl-based MTDLs that were synthesized using an optimized microwave-assisted Suzuki coupling reaction. In addition, the results for the most potent dual inhibitor **4d** identified in this study from the in vitro plasma stability assays in human and rat plasma, and *in vivo* tests of acute inflammatory pain are presented.

2. Results and discussion

2.1. Design, synthesis, and biological evaluations of quinolinyl-based MTDLs

Our previous SAR studies [22–24] determined that a phenyl ring linked to a central amide-piperidine moiety, which connects to the sulfonamide bond to an aromatic ring, represents a crucial feature for the potent dual inhibition at both enzymes (green box, Fig. 2). Numerous substitutions were tested on the right side (blue circle, Fig. 2) of the scaffold. So far, the left side of the molecule is not well-explored, but a few studies pointed out that a bulky, hydrophobic aromatic or cycloalkyl moieties (such as benzothiazole and

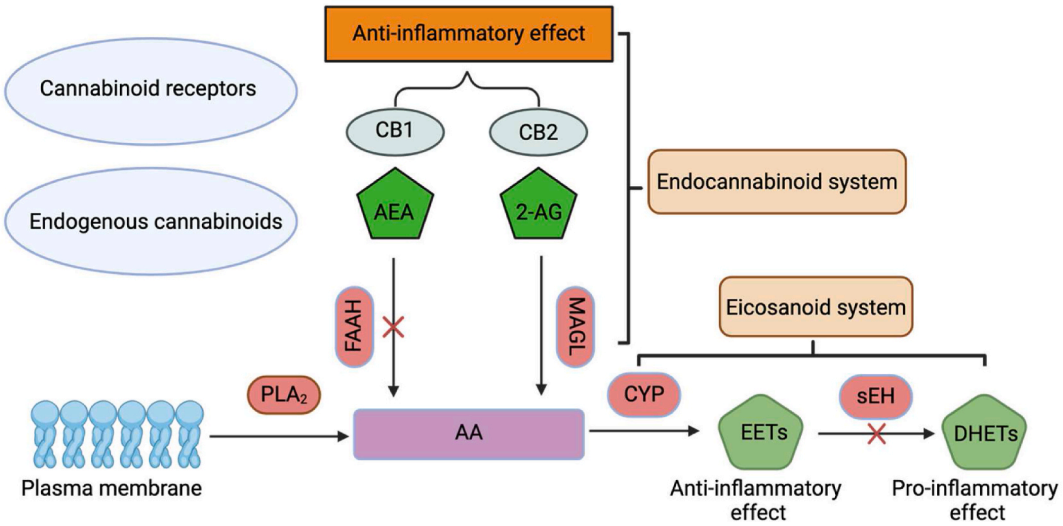

Fig. 1. Metabolic pathways of arachidonic acid and endocannabinoid system. During inflammation the enzyme phospholipase A2 (PLA2) releases long chain fatty acids such as arachidonic acid (AA), which is further metabolized via Cytochrome P450 (CYP) epoxygenases into epoxyeicosatrienoic acids (EETs) and other epoxy fatty acids which possess analgesic and anti-inflammatory properties. EETs are hydrolyzed into pro-inflammatory dihydroxyeicosatrienoic acids (DHETs) via sEH pathway. Anandamides, endogenous cannabinoids with analgesic properties are hydrolyzed by FAAH into arachidonic acid.

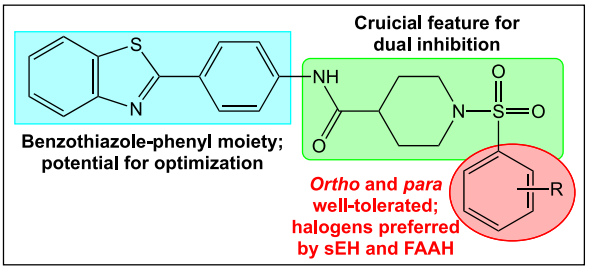

Fig. 2. Previous SAR and design strategy.

4-phenylthiazole) are important for the inhibition of both enzymes. In this study, we examined the importance of the benzothiazole ring on the dual sEH/FAAH inhibition, by incorporating the quinoline ring on the left side of the molecule. The benzothiazole ring and its derivatives are known for their anti-inflammatory and analgesic activities and are an important part of many medicinal chemistry and drug discovery studies [26–28]. However this heterocyclic ring is hydrophobic and weakly basic [29], which contributes to low solubility which in turns limits their pharmacological application. On the other hand, the quinoline moiety is also well-utilized moiety in drug discovery, medicinal chemistry in general, and is present in many FDA-approved drugs. This scaffold is also known for its wide range of pharmacological effects, such as anticancer, anti-inflammatory, antimalarial, antibacterial, and other activities [30]. The quinoline ring is a bulky, hydrophobic moiety, which is important for the activity at both FAAH and sEH, but is more polar and more basic than benzothiazole ring and it can be formulated as a salt, which should dramatically increase its solubility. In addition, quinoline ring (if active) could offer access to many polar and nonpolar chemical substituents/groups that could improve sEH and FAAH inhibition in the follow-up SAR studies. Overall, successful replacement of the benzothiazole with a quinoline ring could provide a new lead compound with the potentially improved pharmacokinetic properties.

Following the synthetic procedure shown in Scheme 1, the commercially available 2-chlorobenzenesulfonyl chloride and methyl isonipecotate were first coupled using triethylamine and microwave irradiation for 20 min at 80 °C. Compound **1** was obtained in 78 % yield. Removal of the methyl ester group with a saponification reaction using 2 M aqueous solution of lithium hydroxide, afforded a carboxylic acid intermediate **2** in ~80 % yield. Next, the same EDC-peptide coupling methodology previously described by us [24], provided a key intermediate, of a boronic acid-pinacol ester **3** in 65 % yield. At this stage, our plan was to implement a direct coupling of **3** with various bromoquinolines using the Suzuki-Miyaura reaction. The previously published Suzuki-Miyaura reaction procedures include microwave-assisted irradiation, which produced more efficient product yields and should be environmentally friendly by increasing its efficiency and decreasing the probability of any byproducts [31,32]. After some optimization of reaction conditions, the best direct biaryl cross-coupling was obtained using microwave irradiation for 60 min at 110 °C, tetrahydrofuran/water (4:1) mixture as a solvent, potassium carbonate as a base and palladium-tetrakis(triphenylphosphine) as a catalyst. Using seven different bromoquinolines, the target analogs **4a-g** were obtained in moderate to high yields, 25–91 %.

All synthesized analogs **4a-g** were subsequently evaluated for their inhibitory potency against human FAAH, and human, mouse, and rat sEHs (Table 1). The introduction of the bulky, aromatic quinoline ring was very well-tolerated at both FAAH and sEH enzymes, compared to benzothiazole ring (**SP 4–5**) with the comparable inhibition potency in low nanomolar range for the human FAAH and sEH enzymes, and yielding even more potent inhibitors for the rat sEH. The IC_{50} values obtained in the human FAAH inhibition assay showed that orientation of the quinoline ring does affect the potency. Namely, **4b** (3-quinolinyl) and **4g** (8-quinolinyl) analogs were less efficient in inhibiting FAAH compared to other analogs, especially compared to the analog **4a** (2-quinolinyl) which was the most

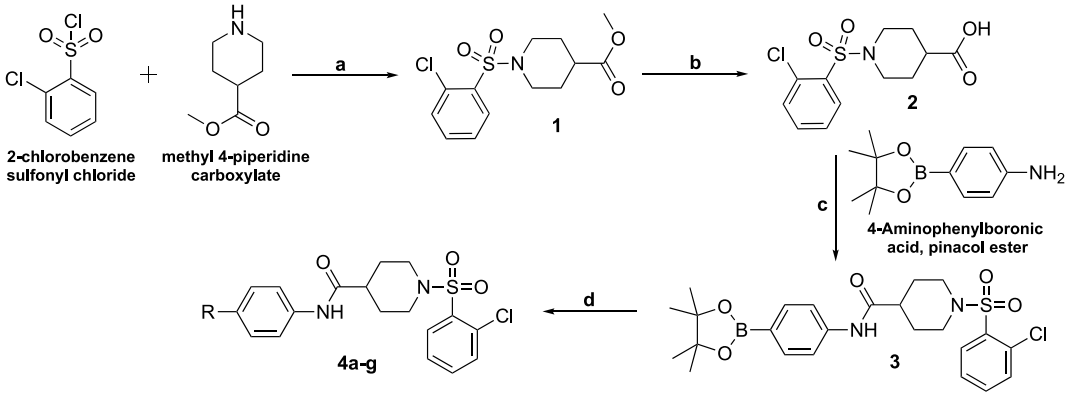

Scheme 1. *Reagents and conditions:*(a) Et_3N, CH_2Cl_2, 20 min, 80 °C, microwave irradiation, 78 %; (b) 4.6 M aq LiOH; THF/H_2O, 16 h, rt, 78 %; (c) EDC, DMAP, CH_2Cl_2, 20 min, 80 °C, microwave irradiation, 65 %; (d) R–Br (see Table 1for R),$Pd(PPh_3)_4$; K_2CO_3, THF/H_2O, 60 min, 110 °C, microwave irradiation, 25–91 %.

Table 1
Fatty acid amide hydrolase (FAAH) and soluble epoxide hydrolase (sEH) inhibitory activities.

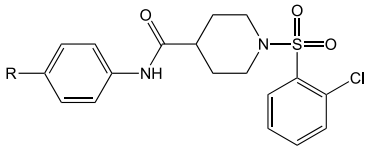

Compound	R	Human FAAH IC_{50} (nM)[a]	Human sEH IC_{50} (nM)[a]	Mouse sEH IC_{50} (nM)[a]	Rat sEH IC_{50} (nM)[a]
URB597[b]	–	35	–	–	–
t-TUCB[c]	–	–	0.3	1.6	9.1
SP 4–5	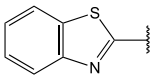	7.0	9.6	812.8	3.9
4a	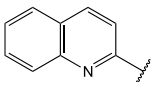	3.5	35.3	181.9	1.4
4b	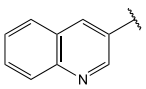	16.0	10.6	116.5	2.5
4c	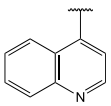	88.7	1.0	28.6	0.7
4d	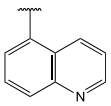	19.6	1.7	17.2	2.0
4e	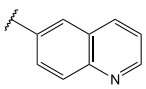	50.8	5.4	87.7	1.6
4f	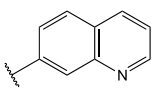	10.5	9.6	38.2	8.1
4g	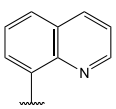	134.7	5.0	95.9	0.8

[a] Reported IC_{50} values are the average of three replicates. The assay as performed here has a standard error between 10 and 20 % suggesting that differences of two-fold or greater are significant.
[B] Positive control for FAAH inhibition.
[C] Positive control for sEH inhibition.

potent FAAH inhibitor identified in this study with the IC_{50} value of 3.5 nM. Previously, **SP 4–5** and other benzothiazole dual inhibitors were very potent inhibitors of human and rat sEH enzyme, but weak inhibitors of mouse sEH [24]. However, the positive control sEH inhibitor, *t*-TUCB, is active in the enzymes from all three species (Table 1). Since the sequence alignment of human, mouse, and rat sEH enzymes is high (>70 %), and there are many reported sEH inhibitors that are active in human, rat and mouse enzymes, we hypothesized that these significant species differences might be due the interactions between the active site of sEH and specific chemical groups present in our library of dual inhibitors. Indeed, this set of quinolinyl-based MTDLs is active in all three, human, mouse, and rat sEH inhibition assays, suggesting that the benzothiazole moiety, and its interaction with the amino acid residues located in the active site of mouse sEH could be the reason why the previous benzothiazole library of analogs performed significantly weaker in the mouse enzyme inhibition sEH assay. Since all quinolinyl analogs were active on both FAAH and sEH, this SAR study suggests that enhanced potency of analogs **4a-g**, is probably due to basicity from the nitrogen atom, but not due to the location of the nitrogen atom within the quinoline ring and the overall 3D orientation of the whole molecule, i.e. the binding pockets of both enzymes can successfully fit bulky groups located on the left side of the molecule.

We decided to further examine MTDL **4d** *in vivo*, since it shows the best potency profile in all inhibition assays, i.e. having IC_{50} values of 19.6 nM in human FAAH, and 1.7 nM, 17.2 nM and 2.0 nM in human, mouse and rat sEH, respectively. We first wanted to determine the mode of the inhibition of **4d** (i.e., if it inhibits FAAH in reversible or irreversible manner). It has been previously shown that URB597 operates as an irreversible inhibitor [33], making the covalent bond with S241, while we reported that the benzothiazole analog **SP 4–5** might be a reversible inhibitor [23]. One approach to elucidate the mode of the inhibition is to perform the time-dependent inhibition experiment, where the inhibitor is preincubated with FAAH at various times (e.g. 5 and 60 min), and if the potency increases over the time (IC_{50} value decreases), one can conclude that the compound inhibits the enzyme via the irreversible mechanism, while if the inhibition potency does not change significantly, the compound is likely a reversible inhibitor. This method has been used to determine mechanism of inhibition in many previous settings [34,35]. In our hands, the inhibition potency of **4d** did not significantly change over time (Supplemental, Table S1), similar to **SP 4–5**, while the control URB 597 shows increase in potency over the same time period. These data suggest that **4d** binds to and inhibit FAAH in a similar manner as **SP 4–5**, i.e. as a reversible inhibitor.

2.2. *In vitro plasma stability studies*

Several non-specific esterases and amidases present in plasma and rapidly degrade compounds drugs containing amide, ester, sulfonamide, and some other functional groups which leads to poor *in vivo* results. Since this set of compounds possess both amide and sulfonamide groups, **4d** was tested in a plasma stability assay before we proceeded with *in vivo* tests. There are also reported relevant species differences in plasma stability, thus plasma stability assays were performed with both human and rat plasma. The stability profiles for **4d** and three known test compounds are summarized in Table 2 and Figs. S10–S13. The results revealed that there is a significant difference in the stability of the compound **4d** in the plasma of human vs. rat, i.e. compound is much more stable in human plasma than in rat plasma. However, **4d** outperformed a known FDA-approved drug warfarin that was used as a negative control, due to increased stability in plasma. It had a longer half live than warfarin in both rat and human plasma stability assays. This assay does not predict the absorption and the distribution of the drug, but in terms of the stability, **4d** is a good, stable candidate for further testing *in vivo*.

2.3. *Molecular modeling studies*

Encouraged by the results obtained in biological assays, we decided to further explore the binding modes of this set of analogs by performing molecular modeling studies. Since the crystal structure of human FAAH is not available, a homology model of human FAAH was built using the X-Ray crystal data obtained for a small molecule inhibitor bound in the humanized rat FAAH active site (PDB code: 3LJ6) as a template [36]. This particular template is interesting because it contains six mutations in the active site that represent conserved residues in the human enzyme. All quinolinyl-based analogs **4a-g** were successfully docked, however, only the binding profile of the best MTDL **4d** is described here. The catalytic triad of FAAH is composed of three amino acid residues, K142, S217, and S241 [13]. Our docking experiments suggest that **4d** binds in the proximity of the catalytic triad (Fig. 3, blue-labeled residues), with the quinoline moiety orientated towards catalytic site, while the 2-chlorophenyl part is exposed to the solvent.

Interestingly, several amino acid residues, M191, Q273, F192, C269, and V270 are making favorable hydrophobic interactions with the quinolinyl ring of **4d** (Fig. 4A; Fig. 4B - green shading and green ellipses), while S190 makes van der Waals interactions (Fig. 4A; Fig. 4B - gray shading and gray ellipses). Next, the phenyl ring attached to the quinoline moiety makes a non-covalent interaction with the I238 and van der Waals contact with the hydrophobic amino acid residue V276. In addition, the oxygen atom of the amide bond in **4d** is engaged in the hydrogen bonding with the L278, while piperidine and 2-chlorophenyl rings make van der Waals contacts with N259, E274, D306, and S264. Additionally, several residues, K263, S262, R277, T308, and V309 are making favorable non-covalent interactions with these two moieties. All residues, contacts, distances, and types of interactions are summarized in Table 3A.

On the other hand, the crystal structure of human sEH complexed with the amide-piperidine-based inhibitor was previously reported [15]. The crystal structure reveal that the hydrolysis binding site is located close to the C-terminus domain and is composed of a long hydrophobic pocket, where epoxy fatty acid substrates are biding. We hypothesized that amide-based sEH inhibitors bind to it with high potency because they mimic an epoxide ring opening transition-state. Moreover, the amide moiety of the sEH inhibitor is in the proximity of the catalytic triad, Y383–Y466-D335, and has potential to establish hydrogen bonds with these amino acid residues. The docking experiments of this set of analogs are consistent with our X-Ray crystal data and are exemplified with the MTDL **4d** (Fig. 5).

Table 2
The in vitro half-lives ($t_{1/2}$) of the compound **4d**, Warfarin, Propantheline and Enalapril and in human and rat plasma.

Compound	Test Species	Matrix	Half-life $t_{1/2}$ (min)	Comments
4d	Human	Plasma	436	
Warfarin	Human	Plasma	304	Negative control
Propantheline	Human	Plasma	11.3	Positive control
4d	Rat	Plasma	176	
Warfarin	Rat	Plasma	159	Negative control
Enalapril	Rat	Plasma	6.44	Positive control

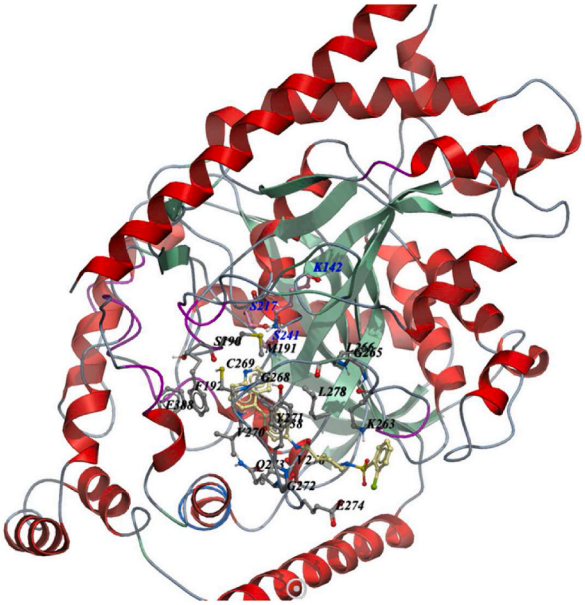

Fig. 3. Orientation of **4d** in FAAH enzyme. The quinolinyl-moiety is orientated next to the catalytic triad (K142–S217–S241), labeled in blue. The 2-chlorophenyl group is facing the entrance of the binding site. Ligand **4d** is displayed in yellow stick.

According to the proposed binding mode of **4d**, the first hydrogen bond is present between Y383, which acts as a hydrogen bond donor (HBD), and the carbonyl oxygen of the of **4d**, which represents a hydrogen bond acceptor (HBA). The second hydrogen bond is observed between D335 (the oxygen atom on this amino acid residue is a HBA), and the nitrogen hydrogen of **4d** (acting as a HBD), with the proposed distance of 2.6 Å (Fig. 6A; 6B – dotted lines, blue ellipses). Several van der Waals contacts are observed: the phenyl ring adjacent to quinoline moiety interacts with Q384, while the 2-chlorophenyl moiety is making van der Waals contacts with L408, R410, S412, D496 and F497 (Fig. 6A; 6B – gray shading and gray ellipses). There are numerous other non-covalent interactions, which are shown in green ellipses and green shading: quinoline ring interacting with the hydrophobic parts of residues M339 and L499, phenyl ring next to the quinoline moiety making π-π contacts with W336 and Y466, piperidine ring interacting with F267, M419, L417, and H524, and finally, 2-chlorophenyl ring making a π-π interaction with W525 and a hydrophobic interaction with V498. All residues, contacts, distances, and types of interactions are summarized in Table 3B. Although quinoline part of the molecule is orientated deep into the hydrophobic part of the sEH catalytic site, there is still an open surface (represented with a broken line in Fig. 6B) beneath it, suggesting that some more complex nitrogen-containing moieties could potentially fit in this pocket such as isoquinolines, pyrimidines, quinoxaline, quinazolines, etc.

2.4. In silico ADMET predictions and NIHM PDSP evaluation of SP 4-5

As a part of our drug design process, several important pharmacokinetic and pharmacodynamic properties were calculated for the quinolinyl-based library of compounds, **4a-g**, and performed comparative analysis with **SP 4–5**, a previously identified dual FAAH/sEH inhibitor [22–24], and known FAAH and sEH inhibitors, URB597 and t-TUCB, respectively (Table 4).

According to the *Lipinski Rule of Five* [37], most drugs that have a good oral bioavailability do not violate more than one of the following rules: molecular weight is below 500 g/mol, logP is less than 5, drug should not have more than 10 hydrogen bond acceptors (HBA) and should not have more than 5 hydrogen bond donors (HBD). Compared to our lead compound **SP 4–5**, all quinoline-based analogs have lower molecular weight and are just slightly above 500 g/mol. Just one analog, **4a**, has calculated logP value above 5, while analog **4d** has the lowest logP and this is one more reason why this compound was selected for *in vivo* evaluation (see above). It has been shown previously that compounds possessing high melting points coupled with high lipophilicity (logP>5) contribute to poor solubility and low oral absorption [38]. Interestingly, placement of nitrogen into the second quinolinyl ring significantly decreased the melting points, but even these numbers are high for potential formulation. Thus, future SAR studies should focus in exploring functional groups that can be added to quinolinyl ring with the aim to further decrease the melting points of this series while obtaining compounds that are highly potent and less lipophilic. None of the analogs tested, **4a-g**, are exceeding 10 HBA and 5 HBD.

Another commonly used set of rules, *Veber's rule* [39] predicts that poor absorption or permeation is more likely linked to polar surface area (PSA) and the number of rotatable bonds of the drugs, rather than the size of the molecule, i.e. molecular weight. According to this rule, molecules that possess PSA below 140 $Å^2$ and less than 10 rotatable bonds should have a good oral bioavailability. All newly synthesized quinoline-based MTDLs are not violating neither of *Veber's rules* (Table 4). These positive predictions suggest that this set of analogs, and specifically our new lead compound **4d**, could be applied orally to animal models in the future.

The compounds described herein are designed to not cross the Blood Brain Barrier (BBB), because we hypothesized that the

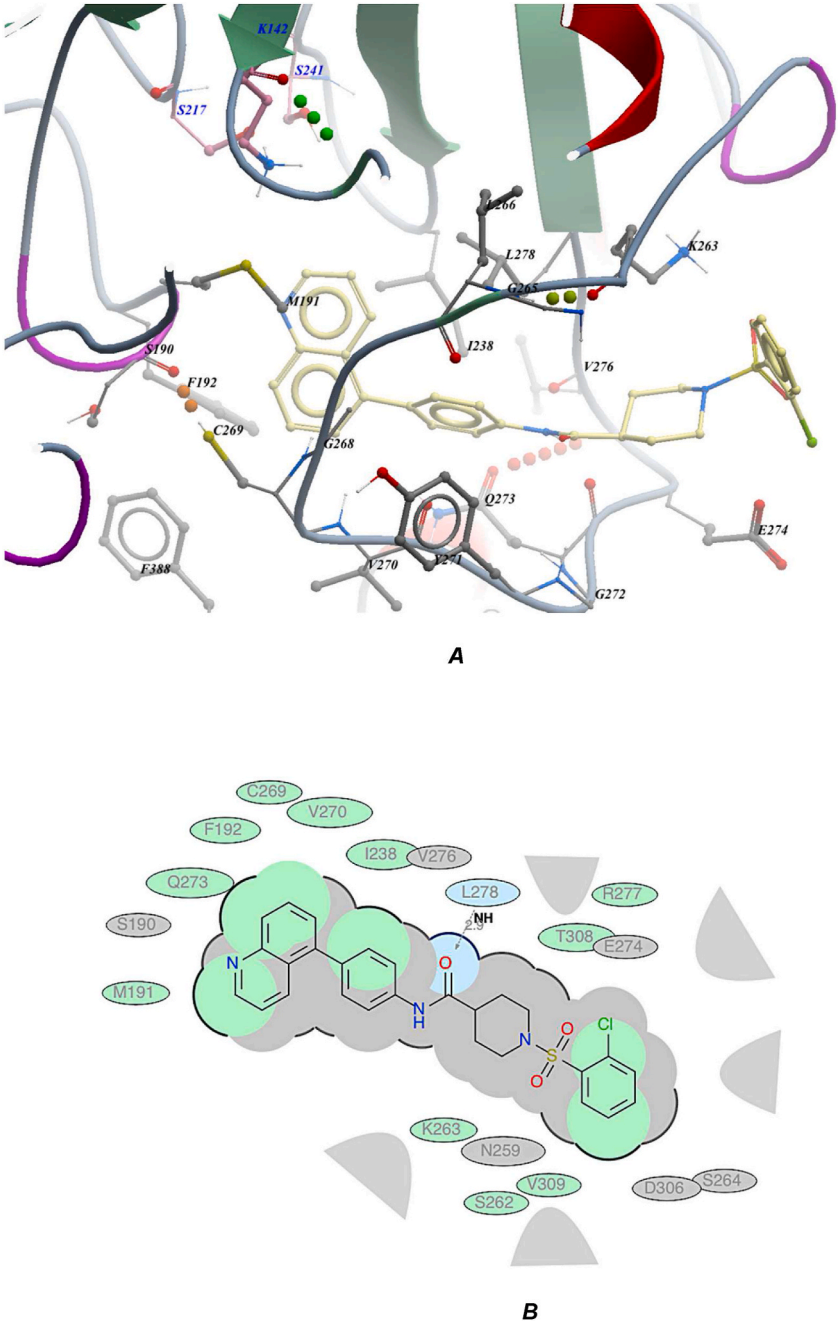

Fig. 4. A3D representation of **4d** docked in the binding pocket of the human FAAH homology model (3D representation) with the important amino acid residues in the proximity of the **4d**. Ligand **4d** is displayed in yellow stick.
Fig. 4B. 2D representation of **4d** in the active site of the human FAAH homology model: in green are shown possible hydrophobic interactions; gray shading represents vdW interactions; gray parabolas are showing open accessible surfaces areas in FAAH; blue ellipse and gray dotted line represent a hydrogen bond; broken thick line around **4d** shape indicates accessible surfaces; the proximity of amino acid residues to **4d** is represented by the size of their ellipse, i.e. the smaller ellipse the closer to **4d**, and vice versa.

inhibition of these two enzymes in the peripheral nervous system should be sufficient to provide anti-inflammatory and anti-nociceptive effects. In addition, it would avoid potential binding to opioid receptors located in the central nervous system, which would in turn potentially produce the adverse effects common for the opioid drugs such as sedation, respiratory depression, and death. The Gupta et al. (2019) [40] BBB prediction score, where a BBB score above 4 indicates that the tested compound can pass the BBB, was used as one of our drug design tools (Table 4). None of the newly synthesized analogs are predicted to penetrate the BBB, and thus one should not expect any unwanted CNS-related side effects and/or binding to opioid receptors.

Table 3A
The list of hydrogen bonds and hydrophobic interactions of ***4d*** *docked in human FAAH with the distances from amino acid residues.*

Amino acid residue	Type	Distance (Å)
L278	H-bond	2.91
M191	Hydrophobic	3.79
F192	Hydrophobic	3.34
I238	Hydrophobic	3.14
S262	Hydrophobic	4.44
K263	Hydrophobic	3.95
C269	Hydrophobic	4.33
V270	Hydrophobic	3.53
Q273	Hydrophobic	3.95
R277	Hydrophobic	4.41
T308	Hydrophobic	3.58
V309	Hydrophobic	4.38

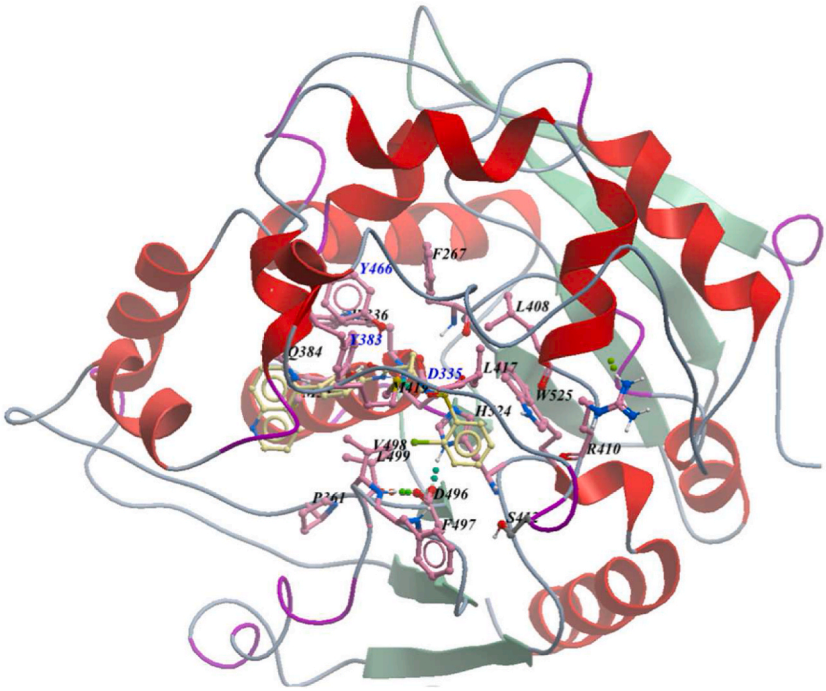

Fig. 5. Orientation of **4d** in sEH enzyme. The amide is located in the proximity of the catalytic triad (Y383–Y466-D335), labeled in blue. The 2-chlorophenyl group is facing the entrance of the active site. Ligand **4d** is displayed in yellow stick.

However, some chemicals do not obey the BBB predictions from Gupta et al. (2019) [40] method, and could potentially cross the BBB using protein transporters or transcellular transport (pinocytosis) and bind to opioid receptors. Our previously described dual FAAH/sEH inhibitor **SP 4–5** has a BBB score value of 1.8 (Table 4) suggesting that this compound should not cross the BBB. Because some of its *in vivo* effects could result from binding to opioid receptor [23], **SP 4–5** was tested by NIHM PDSP for its ability to bind (either inhibit or activate) three different opioid receptor subtypes: delta (DOR), kappa (KOR) and mu (MOR). As shown in Table 5, **SP 4–5** did not significantly bind to any of the three receptors tested, confirming that even if **SP 4–5** crosses BBB, the analgesic effect produced is not from stimulation of any of these 3 receptors. Importantly, this lack of activity of **SP 4–5** may be particularly advantageous to avoid any opioid-related side effects mediated by the central nervous system (e.g., sedation, respiratory depression, addiction). Because the series of compounds described herein **4a-g**, are structurally related in part to **SP 4–5**, it is unlikely that these compounds bind to the tested opioid receptors also.

The microsomal liver stability assay (MLA) represents a good predictor for *in vivo* metabolism preliminary pharmacokinetic properties. Here, the $MLAt_{1/2}$ for the quinolinyl-based analogs were predicted (Table 4). The values for **4a-g** are close to the predicted value of **SP 4–5** (around 30 min), which is close to the experimentally determined value (18.1 min) for this compound. Hence, **4a-g** stability in liver microsomes should be more or less similar to **SP 4–5**.

Next, a pharmacokinetic prediction was to evaluate the half-life of this series of compounds in plasma. The half-life of a drug

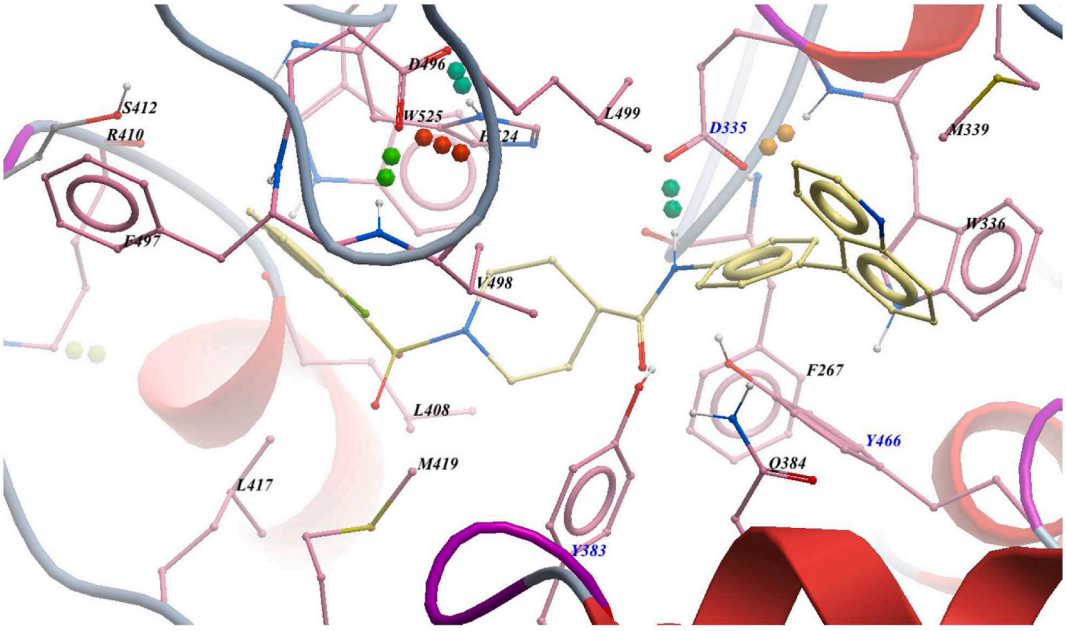

A

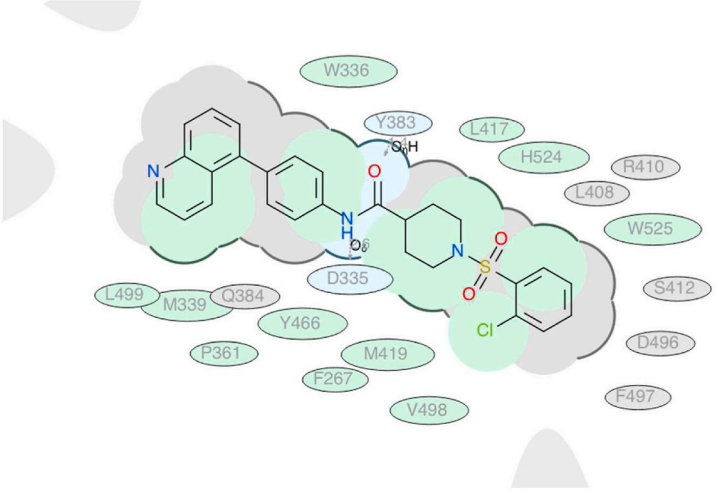

B

Fig. 6. A. Binding of **4d** in the active site of the human sEH model derived from the PDB: 4HAI (3D representation) with the important amino acid residues in the proximity of the **4d**. Ligand **4d** is displayed in yellow stick.
Fig. 6B. 2D representation of **4d** in the active site of the human sEH model derived from the PDB: 4HAI: in green are shown possible hydrophobic interactions; gray shading represents vdW interactions; gray parabolas are showing open accessible surfaces areas in sEH; blue ellipse and gray dotted line represent a hydrogen bond; broken thick line around **4d** shape indicates accessible surfaces; the proximity of amino acid residues to **4d** is represented by the size of their ellipse, i.e. the smaller ellipse the closer to 4d, and vice versa.

represents the time that body needs to clear 50 % of the drug in the plasma, i.e. the shorter the half-life is, the higher is the clearance from the body and vice versa. All the quinoline MTDLs have predicted longer half-lives than **SP 4–5** (Table 4). The ICM Pro software predicts the plasma half-life in human plasma, and the prediction half-life for our new lead compound **4d** is 2.6 h (156 min), which is close to the experimentally determined half-life for this compound in rat plasma (Table 4 – half-life for **4d** is 436 min in human and 176 min in rat plasma). This prediction feature was used to compare how different structural changes on the parent molecule will affect

Table 3B
*The list of hydrogen bonds and hydrophobic interactions of **4d** docked in human sEH with the distances from amino acid residues.*

Amino acid residue	Type	Distance (Å)
Y383	H-bond	1.41
D335	H-bond	2.62
F267	Hydrophobic	4.38
W336	Hydrophobic	3.52
M339	Hydrophobic	3.31
P361	Hydrophobic	4.15
L417	Hydrophobic	4.07
M419	Hydrophobic	3.60
Y466	Hydrophobic	3.90
V498	Hydrophobic	3.17
L499	Hydrophobic	3.63
H524	Hydrophobic	2.93
W525	Hydrophobic	3.77

Table 4
Predicted pharmacokinetic and pharmacodynamic properties for URB597, t-TUCB, SP 4–5 and analogs **4a-g**.

Compound	MW	cLogP[a]	HBA[b]	HBD[c]	PSA[d]	nRotB[e]	BBB[f] Score	$t_{1/2}$ hMLA[g](h)	$t_{1/2}$ Plasma (h)	Pro-Inflammation	hERG[h]	$logLD_{50}$
URB597	338.2	4.11	5	3	136.0	6	2.43	0.38	2.14	0	0.21	1.71
t-TUCB	438.1	5.22	7	3	140.1	9	1.70	1.9	3.88	0	0.06	2.64
SP 4–5	511.1	4.93	8	1	118.2	6	1.84	0.52	1.44	0	0.16	1.85
4a	505.1	5.03	8	1	112.7	6	2.15	0.46	3.01	0	0.11	1.58
4b	505.1	4.88	8	1	126.3	6	1.57	0.62	2.32	0	0.19	1.32
4c	505.1	4.68	8	1	123.8	6	1.61	0.50	1.78	0	0.42	1.97
4d	505.1	4.59	8	1	119.5	6	1.96	0.51	2.60	0	0.28	1.96
4e	505.1	4.73	8	1	121.8	6	1.57	0.59	1.77	0	0.16	2.08
4f	505.1	4.72	8	1	119.3	6	1.92	0.56	2.95	0	0.17	2.15
4g	505.1	4.48	8	1	111.6	6	2.09	0.76	3.50	0	0.13	2.14

[a] cLogP – calculated logP (log of the partition coefficient).
[b] HBA – number of hydrogen bond acceptors.
[c] HBD – number of hydrogen bond donors.
[d] PSA – polar surface area.
[e] nRotB – number or rotatable bonds.
[f] BBB – Blood Brain Barrier.
[g] hMLA – human microsomal liver stability assay.
[h] hERG - human ether-a-go-go-related gene.

Table 5
NIHM PDSP screening results for binding of **SP 4–5** to opioid receptor subtypes.

Receptor	Inhibition (%)[a]	$P_{(value=0)}$[b]
DOR	10.5 ± 8.9	0.10
KOR	6.5 ± 3.4	0.03
MOR	4.4 ± 4.3	0.13

[a] Data represent average ± standard deviation of inhibition (n = 4 determinations) for compound **SP 4–5** tested at 10 μM on three opioid receptor subtypes.
[b] Probability that results are equal to zero (no inhibition nor activation (negative inhibition) of the receptor).

the stability in plasma as general guide for the future drug design. However, for potential future preclinical and clinical studies, experimentally obtained $t_{1/2}$ values should be used.

Because we are developing anti-inflammatory drugs, the potential presence of any pro-inflammatory properties was investigated (Table 4). The ICM Pro software model for Pro-Inflammatory predictions is trained on 82158 compounds and defines a score range from 0 to 1, with scores above 0.5 indicating a high probability of being pro-inflammatory. The prediction scores (Table 4) suggest that none of the quinoline-based analogs should be pro-inflammatory.

As part of the toxicity predictions, the hERG score and $logLD_{50}$ value were calculated for each compound described in this study. The inhibition of the hERG potassium channels is linked to the cardiotoxicity of drugs and can cause deadly arrythmias [41]. The ICM Pro model for hERG inhibition has been trained on 2256 compounds, and a score equal or above 0.5 predicts that the tested compound is a hERG (human ether-a-go-go-related gene) inhibitor. All compounds tested showed the hERG score below 0.5, suggesting that none

of new compounds will likely inhibit this receptor significantly.

Finally, we determined the LD_{50}, a dose of a drug that will kill 50 % of the tested animals. The ICM Pro model for this property has been tested on 3992 compounds and expressed as a logarithm of LD_{50} value. A value of 0 represents an LD_{50} value of 1 mg/kg, meaning very toxic, while the value of 2 correlates to LD_{50} value of 100 mg/kg, i.e. a safe drug. The results (Table 4) indicate that almost all of the quinoline-based drugs are close or above $logLD_{50}$ value of 2, suggesting that these compounds should have a high LD_{50} values and thus have low toxicity.

2.5. In vivo evaluation of 4d

The Formalin Test has been used to determine the antinociceptive and anti-inflammatory effects of drugs [42]. Biphasic inflammatory pain is generated by injecting dilute formalin into the plantar surface of the hind paw of the lightly anesthetized rat. The resulting pain-related behavioral response, typically licking of the injected paw, is measured in 5 min intervals for 60 min to determine the magnitude of pain and subsequent antinociception. The Formalin Test is separated into two phases. Phase 1 is approximately 0–10 min after injection and the resulting pain is a result of a direct activation of nociceptors. Phase 2 is approximately 20–60 min after hind paw injection, and this pain is mediated primarily by inflammatory mechanisms in the peripheral nervous system along with changes in the dorsal horn of the spinal cord, an important area for pain processing [42].

Here, male rats were pre-treated with 1 mg/kg **4d,** 30 mg/kg ketoprofen (nonsteroidal anti-inflammatory drug) or vehicle (i.e., no drug) 30 min prior to injection of formalin. This dose of **4d** was chosen based on our previous findings that 1 mg/kg of **SP 4–5** inhibits pain and does not produce locomotor side effects in rats [23,43].

Fig. 7A shows the time spent licking the injected paw over the entire 60 min testing period following hind paw injection of formalin, which is 30–90 min after injection of **4d**, ketoprofen, or vehicle. Fig. 7B shows the area under the curve over the same period for each group. A one-way analysis of variance revealed that pain behaviors in animals pre-treated with **4d** or ketoprofen differed compared to animals treated with vehicle [$F(2, 180) = 6.26$, $p = 0.002$]. A Tukey post-hoc test revealed that **4d**-treated animals ($p < 0.01$ vs. vehicle) and ketoprofen-treated animals ($p < 0.05$ vs. vehicle) licked the injected paw for significantly less time than vehicle-treated rats. There were no significant differences in the time spent licking in **4d**- and ketoprofen-treated rats ($p > 0.05$).

This effect is likely primarily driven by behavioral changes in Phase 2 of the Formalin Test (Fig. 7A), which may indicate the mechanism of action of **4d**. Centrally acting analgesics such as opioids typically inhibit pain-related behaviors in both Phase 1 and

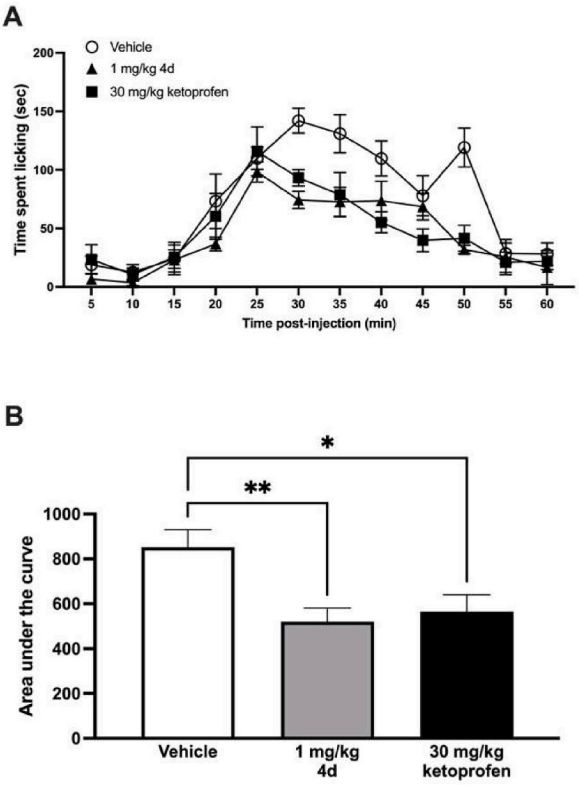

Fig. 7. Administration of **4d** inhibits pain-related behavior after a hindpaw injection of dilute formalin. (A) The time spent licking the injected hindpaw is presented for the entire 60 min testing period. (B) Area under the curve analysis for the time spent licking is presented. * indicates $p < 0.05$; ** indicates $p < 0.01$.

Phase 2 [44]. The immediate behavioral responses after hind paw injection of formalin (i.e., Phase 1) are similar across groups indicating that **4d** may not work to inhibit pain via central mechanisms. This may mean that **4d** is interrupting or preventing inflammatory processes in the periphery to produce antinociception in this test. The lack of BBB penetration of our other MTDLs (see *In silico ADMET predictions section*) further supports this hypothesis.

3. Conclusion

New quinolinyl-based dual sEH/FAAH potent inhibitors are reported. Seven potent dual inhibitors were synthesized using a microwave-assisted Suzuki-Miyaura coupling reaction. This optimized reaction will be used in future follow-up studies to generate other heterocyclic moieties such as quinoline-substituted rings, isoquinoline and its derivatives, quinoxaline and quinazoline rings. The quinoline ring is more polar and more basic compared to benzothiazole ring, which is a very weak base, and this property will allow us to prepare a salt form of **4d** which should improve the solubility. Our SAR study shows that the quinolinyl group is well tolerated in human FAAH, and human, rat and mouse sEH enzyme binding sites, yielding nanomolar inhibitors. Previous 4-phenylthiazole [23] and benzothiazole [24] dual inhibitors were not active in mouse sEH inhibition assays. Three quinoline analogs (**4c**, **4d** and **4f**) are very potent and other are moderately potent in mouse sEH which will allow this set of analogs to be further tested in mouse models of pain. Molecular modeling studies suggest that left side of the molecule can further be modified with bulky aromatic groups. Compound **4d** (with IC_{50} values of 19.6 nM in human FAAH, and 1.7 nM, 17.2 nM and 2.0 nM with human, mouse, and rat sEH enzymes, respectively) was selected for further evaluation in a plasma stability assay and *in vivo* in a test of acute inflammatory pain. *In vitro* stability assay in plasma determined half-lives in human and rat plasma to be 436 and 176 min, which were longer than warfarin, the negative control (304 and 159 min, respectively). *In vivo* study revealed that 1 mg/kg **4d** can inhibit acute inflammatory pain in male rats to a similar degree as the traditional nonsteroidal anti-inflammatory drug ketoprofen (30 mg/kg) after intraperitoneal injection. In addition, we report that one of our previously identified dual inhibitor **SP 4–5** (possessing the same pharmacophore as the quinolinyl-based analogs) does not interact with opioid receptors. Together, these results highlight the potency of dual FAAH/sEH Multitarget-Directed Ligands to treat pain without the deleterious addiction effects associated with opioid treatments.

4. Materials and methods

All reagents and solvents were commercially available and used without further purification. Reactions were monitored by thin-layer chromatography (TLC) performed on silica gel 60 F254 precoated aluminum plates (Sigma–Aldrich: 105549). Flash chromatography was carried out on the Teledyne CombiFlash Rf + Separation System. Purity of each compound is above 95 % which is determined by TLC, LC-MS, and proton and carbon NMR. ^{1}H and ^{13}C NMR spectra were recorded with a Bruker Avance-II 400-MHz broadband multinuclear system (400 MHz for ^{1}H and 101 MHz for ^{13}C) in $CDCl_3$ or DMSO-d_6 with tetramethylsilane as an internal reference. Proton NMR spectra are reported in parts per million (ppm) relative to the signals for chloroform (7.26 ppm) or dimethylsulfoxide (2.50 ppm). Carbon NMR spectra were reported in ppm relative to the signals for chloroform (77.2 ppm) or dimethylsulfoxide (39.5 ppm). Proton chemical shifts (δ ppm) were reported as follows: multiplicity (s = singlet, bs = broad singlet, d = doublet, t = triplet, q = quartet, m = multiplet). HRMS analysis was performed on a Thermo Scientific Q Exactive Focus Orbitrap LC-MS/MS System with LC grade solvents. The measurements were run in positive ion mode. Microwave reactions were carried out in a CEM 2.0 Discover microwave synthesizer. Melting points were measured with a DigiMelt MPA-160 melting point apparatus and are reported uncorrected. Fatty Acid Amide Hydrolase (human, recombinant) was purchased from Cayman Chemical and Soluble Epoxide Hydrolase (human, mouse, and rat, recombinant) was obtained from UC Davis. Fig. 1 and graphical abstract were created with BioRender.com. Molecular modeling studies, docking experiments and prediction of ADMET were performed using ICM Pro Molsoft software.

5. Chemistry

5.1. General procedure for the preparation of qunolinyl-phenyl analogs

2-chlorobenzenesulfonyl chloride (2.37 mmol), methyl 4-piperidinecarboxylate (2.37 mmol) and triethylamine (7.11 mmol) were mixed in anhydrous dichloromethane (20 mL) and were subjected to microwave irradiation at 80 °C for 20 min. The organic layer was transferred to separatory funnel, washed with an aqueous solution of saturated sodium bicarbonate (50 mL), separated, dried over anhydrous sodium sulfate, filtered, and concentrated. The crude product, a yellowish oil, was purified using a CombiFlash system with following parameters: 0–50 % ethyl acetate, 100-50 % hexane, over 15 min. The sulfonamide intermediate (ethyl 1-((2-chlorophenyl) sulfonyl)piperidine-4-carboxylate) **1** was obtained as a yellowish thick oil in the amount of 0.59 g (78 % yield). Next, a stirred solution of **1** (1.85 mmol) in tetrahydrofuran (5 mL) was treated with a 4.6 M aqueous solution of lithium hydroxide (6 mL) and the reaction was stirred overnight at room temperature. The progress of the reaction was monitored with TLC. Upon completion, the solvents are removed in vacuo, followed by addition of ethyl acetate (25 mL) and water (5 mL). The mixture was then cooled to 0 °C in an ice bath, stirred vigorously, and 6 N HCl was added dropwise, until pH~2 (checked with pH paper). The organic layer was transferred to the separatory funnel, separated, dried over anhydrous sodium sulfate, filtered, and concentrated in vacuo. The crude product was recrystallized in hexane, and carboxylic acid **2** was obtained as a white solid (0.44 g, 78 % yield). Next, 1.39 mmol of **2**, 2.09 mmol of 1-ethyl-3-(3-dimethylaminopropyl) carbodiimide (EDC), 2.09 mmol of 4-aminophenylboronic acid pinacol ester, and a catalytic amount of 4-dimethylaminopyridine (DMAP) were dissolved in 20 mL anhydrous dichloromethane and subjected to microwave irradiation at

80 °C for 20 min. The organic layer was washed with 1 N HCl (50 mL), followed by aqueous solution of saturated sodium bicarbonate (50 mL). The organic layer was transferred to the separatory funnel, separated, dried over anhydrous sodium sulfate, filtered, and concentrated in vacuo. The crude product was purified by flash chromatography using a CombiFlash system with following parameters: 0–50 % ethyl acetate, 100-50 % hexane, over 20 min and **3** was obtained as a white solid (0.46 g, 65 % yield). Next, 0.20 mmol of **3**, 0.40 mmol of corresponding bromoquinoline, and 0.50 mmol of potassium carbonate were dissolved in a mixture of tetrahydrofuran (1.6 mL) and water (0.4 mL). Upon the addition of 0.010 mmol of palladium-tetrakis(triphenylphosphine), the solution was subjected to microwave irradiation at 110 °C for 60 min. The solvent was removed under reduced pressure and the residue was dissolved in dichloromethane (50 mL) and water (25 mL). The organic layer was transferred to the separatory funnel, separated, dried over anhydrous sodium sulfate, filtered, and concentrated. The crude product was purified using a CombiFlash system with following parameters: 0–50 % ethyl acetate, 100-50 % hexane, over 20 min and final products **4a-g** were obtained in moderate yields (*see Experimental for more details*).

5.2. Measurement of inhibitor potencies on sEH and FAAH

The reported IC_{50} values were obtained using previously published FAAH and sEH fluorescent-based assays [45,46]. The substrate for FAAH inhibition assay *N*-(6-methoxypyridin-3-yl) octanamide (OMP), was synthesized following a previously reported synthetic procedure and reaction conditions [18]. The substrate cyano(6-methoxynaphthalen-2-yl)methyl((3-phenyloxiran-2-yl)methyl) carbonate (CMNPC) for sEH inhibition assay was synthesized at UC Davis (BDH Lab).

FAAH Inhibition Assay: Measurement of human FAAH inhibition potency was done using the substrate OMP ($[S]_{final} = 50$ μM) in sodium phosphate buffer [0.1 M, pH = 8, and 0.1 mg/mL bovine serum albumin (BSA)]. Progress of the reaction was measured by fluorescence detection of 6-methoxypyridin-3-amine at an excitation wavelength of 303 nm and an emission wavelength of 394 nm at 37 °C by the use of a microplate reader M2 (Molecular Devices., CA, USA).

sEH Inhibition Assay: The substrate CMNPC ($[S]_{final} = 5$ μM) was added to wells containing sEH (~2 nM mouse sEH, ~1 nM rat sEH, or ~1 nM human sEH) in sodium phosphate buffer (0.1 M, pH = 7.4 and 0.1 mg/mL BSA, and formation of the fluorescent 6-methoxynaphthaldehyde ($\lambda_{excitation} = 330$ nm, $\lambda_{emission} = 465$ nm, 37 °C) was measured by the use of a microplate reader M2 (Molecular Devices., CA, USA).

The fluorescence generated by hydrolysis was quantified every 30 s for 10 min, and the linear portion of the curve was used to generate the reaction velocity ($v_{inhibitor}$). Values were subtracted from wells containing no enzyme. Next, the IC_{50} values were quantified by simple linear regression of the log [I] vs. % remaining activity ($v_{inhibitor}/v_{DMSO}$) and determining x when y = 0.50 with at least 2 points on either side of 50 % activity mark. All measurements were the average of triplicates. For all assays, the final DMSO concentration was 2 %.

5.3. Plasma stability

Procedure: Plasma stability tests were conducted by Cyprotex US, LLC (Framingham, MA). **4d** was incubated with human or rat plasma (pH 7.4, ±0.1, adjusted if necessary) at 37 °C. At 0, 15, 30, 60, and 120 min, an aliquot was removed from each experimental reaction and mixed with ice-cold stop solution (an acetonitrile containing an analytical internal standard). Stopped reactions were kept on ice for at least 10 min. Samples were filtered by centrifugation for 1 min at 500 rcf and 4 °C, and the supernatants were analyzed by LC-MS/MS.

Analysis: Data were calculated as % parent remaining by assuming 0 min time point peak area ratio (analyte/internal standard) as 100 % and dividing remaining time point peak area ratios by 0 min time point peak area ratio. Data were subjected to fit first-order decay model to calculate slope and thereby half-life:

$$\text{Elimination rate constant } (k) = (-\text{ gradient})$$

$$\text{Half} - \text{life } \left(t_{1/2}\right)(\text{min}) = 0.693 \Big/ k$$

5.4. Molecular modeling

ICM Pro software (Molsoft LLC) was used docking experiments [47]. FAAH inhibitor URB 597, sEH inhibitor t-TUCB, and quinoline analogs **4a–g** were first docked into a homology model of human FAAH enzyme prepared by us previously [18]. Next, a human sEH model was prepared from a crystal structure PDB: 4HAI [15]. In brief, first the PDB file 4HAI was converted to an ICM object and optimized according to the program settings. Next, the inhibitor, N-cycloheptyl-1-(mesitylsulfonyl) piperidine-4-carboxamide, was removed, and binding pockets were identified. For both FAAH and sEH docking experiments were performed following the program guidelines. ICM scores were obtained after this procedure. ICM-Chemist-Pro add on was used for all ADMET predictions to assess URB 597, t-TUCB, SP 4–5 and quinoline analogs **4a-g**.

5.5. In vivo analysis

Subjects: Male Sprague-Dawley rats were purchased from Charles River Laboratories (Hollister, CA, USA) and housed at California

State University, East Bay (Hayward, CA, USA). All rats were at least 50 days old by the start of the study. Rats randomly assigned to treatment groups. Experimenters were blinded to treatment groups. Procedures were approved by the Institutional Animal Care and Use Committee of California State University, East Bay.

Drugs: **4d** and ketoprofen was dissolved in vehicle comprising of 20 % DMSO (Sigma-Aldrich, St. Louis, MO, USA), 20 % Kolliphor® (Sigma-Aldrich, St. Louis, MO, USA), and 60 % normal saline. Drugs were injected intraperitoneally in a volume of 1 mL/kg using a 26-gauge needle. All drugs were administered 30 min prior to hind paw injection of formalin. Rats were immediately returned to their home cages after drug injection.

Formalin Test: Rats were removed from their home cages and briefly anesthetized with isoflurane. Dilute formalin (5 %, 50 μL) was injected into the plantar surface of the right hind paw using a 26-gauge needle. Rats were placed on an elevated mesh rack for observation immediately after hind paw injection. The amount of time spent licking the injected hind paw was measured in seconds in 5 min blocks (300 s per block) for 1 h following hind paw injection.

5.6. Statistical analysis

Data are expressed as mean ± SEM. Data were converted to area under the curve to capture the entire testing period. A one-way analysis of variance was used to evaluate differences. A Tukey post-hoc test was used to further investigate differences between groups. Statistical significance was defined as $p < 0.05$.

Ethics statement

Animal work was done by Dr. Ram Kandasamy's Lab at California State University, East Bay. All procedures were approved by the Institutional Animal Care and Use Committee of California State University, East Bay.

Data availability statement

All data is included in the article, and a supplementary information data file is attached.

CRediT authorship contribution statement

Jeannes Angelia: Investigation, Formal analysis, Data curation. **Leah Duong:** Writing – original draft, Data curation. **Faye Yun:** Writing – original draft, Data curation. **Anesa Mesic:** Investigation, Formal analysis, Conceptualization. **Cassandra Yuan:** Methodology, Investigation, Conceptualization. **Daniel Carr:** Methodology, Investigation. **Siena Gunari:** Investigation, Formal analysis, Conceptualization. **Paula K. Hudson:** Writing – review & editing, Data curation. **Christophe Morisseau:** Writing – review & editing, Formal analysis, Data curation, Conceptualization. **Bruce D. Hammock:** Writing – review & editing, Conceptualization. **Ram Kandasamy:** Writing – original draft, Supervision, Methodology, Investigation, Formal analysis, Data curation, Conceptualization. **Stevan Pecic:** Writing – original draft, Supervision, Software, Methodology, Investigation, Formal analysis, Data curation, Conceptualization.

Declaration of competing interest

The authors declare that they have no known competing financial interests or personal relationships that could have appeared to influence the work reported in this paper.

Acknowledgments

Research reported in this publication was supported by the National Institute of General Medical Sciences of the National Institutes of Health under award number 1 R16GM149204-01. Partial support was provided by NIH – NIEHS RIVER award R35 ES030443-01, and NIH Counter Act award U54 NS127758. The content is solely the responsibility of the authors and does not necessarily represent the official views of the National Institutes of Health. Opioid receptor binding profiles were generously provided by the National Institute of Mental Health's Psychoactive Drug Screening Program, Contract # HHSN-271-2018-00023-C (NIMH PDSP). The NIMH PDSP is Directed by Bryan L. Roth at the University of North Carolina at Chapel Hill and Project Officer Jamie Driscoll at NIMH, Bethesda MD, USA. For experimental details please refer to the PDSP web site https://pdsp.unc.edu/ims/investigator/web/. Faye Yun was supported by the Cal State Fullerton U-RISE at Cal State Fullerton grant 5T34 GM149493-02 from the National Institutes of Health. Instrumentation support was provided by the National Science Foundation MRI (CHE1726903) for acquisition of an UPLC-MS.

Appendix A. Supplementary data

Supplementary data to this article can be found online at https://doi.org/10.1016/j.heliyon.2024.e32262.

References

[1] E. Ricciotti, G.A. FitzGerald, Prostaglandins and inflammation, Arterioscler. Thromb. Vasc. Biol. 31 (5) (2011) 986–1000.
[2] H. Harizi, J.B. Corcuff, N. Gualde, Arachidonic-acid-derived eicosanoids: roles in biology and immunopathology, Trends Mol. Med. 14 (10) (2008) 461–469.
[3] H.C. Lu, K. Mackie, An introduction to the endogenous cannabinoid system, Biol. Psychiatr. 79 (7) (2016) 516–525.
[4] H.C. Lu, K. Mackie, Review of the endocannabinoid system, Biol Psychiatry Cogn Neurosci Neuroimaging 6 (6) (2021) 607–615.
[5] G. Donvito, et al., The endogenous cannabinoid system: a budding source of targets for treating inflammatory and neuropathic pain, Neuropsychopharmacology 43 (1) (2018) 52–79.
[6] J.D. Imig, B.D. Hammock, Soluble epoxide hydrolase as a therapeutic target for cardiovascular diseases, Nat. Rev. Drug Discov. 8 (10) (2009) 794–805.
[7] K. Node, et al., Anti-inflammatory properties of cytochrome P450 epoxygenase-derived eicosanoids, Science 285 (5431) (1999) 1276–1279.
[8] A.A. Spector, et al., Epoxyeicosatrienoic acids (EETs): metabolism and biochemical function, Prog. Lipid Res. 43 (1) (2004) 55–90.
[9] A.A. Spector, A.W. Norris, Action of epoxyeicosatrienoic acids on cellular function, Am. J. Physiol. Cell Physiol. 292 (3) (2007) C996–C1012.
[10] G. Zhang, S. Kodani, B.D. Hammock, Stabilized epoxygenated fatty acids regulate inflammation, pain, angiogenesis and cancer, Prog. Lipid Res. 53 (2014) 108–123.
[11] T. Yang, et al., The role of 14,15-dihydroxyeicosatrienoic acid levels in inflammation and its relationship to lipoproteins, Lipids Health Dis. 12 (2013) 151.
[12] N. Clayton, et al., CB1 and CB2 cannabinoid receptors are implicated in inflammatory pain, Pain 96 (3) (2002) 253–260.
[13] K. Ahn, D.S. Johnson, B.F. Cravatt, Fatty acid amide hydrolase as a potential therapeutic target for the treatment of pain and CNS disorders, Expet Opin. Drug Discov. 4 (7) (2009) 763–784.
[14] S. Pecic, et al., Design, synthesis and evaluation of non-urea inhibitors of soluble epoxide hydrolase, Bioorg. Med. Chem. Lett 22 (1) (2012) 601–605.
[15] S. Pecic, et al., Synthesis and structure–activity relationship of piperidine-derived non-urea soluble epoxide hydrolase inhibitors, Bioorg. Med. Chem. Lett 23 (2) (2013) 417–421.
[16] S. Pecic, et al., Novel piperidine-derived amide sEH inhibitors as mediators of lipid metabolism with improved stability, Prostag. Other Lipid Mediat. 136 (2018) 90–95.
[17] Y. Wang, et al., Inhibition of the soluble epoxide hydrolase as an analgesic strategy: a review of preclinical evidence, J. Pain Res. 14 (2021) 61–72.
[18] S.R. Wilt, et al., Design, microwave-assisted synthesis, biological evaluation and molecular modeling studies of 4-phenylthiazoles as potent fatty acid amide hydrolase inhibitors, Chem. Biol. Drug Des. 95 (5) (2020) 534–547.
[19] B.F. Cravatt, A.H. Lichtman, Fatty acid amide hydrolase: an emerging therapeutic target in the endocannabinoid system, Curr. Opin. Chem. Biol. 7 (4) (2003) 469–475.
[20] O. Sasso, et al., Peripheral FAAH and soluble epoxide hydrolase inhibitors are synergistically antinociceptive, Pharmacol. Res. 97 (2015) 7–15.
[21] S.D. Kodani, et al., Design and potency of dual soluble epoxide hydrolase/fatty acid amide hydrolase inhibitors, ACS Omega 3 (10) (2018) 14076–14086.
[22] S. Wilt, et al., Development of multitarget inhibitors for the treatment of pain: design, synthesis, biological evaluation and molecular modeling studies, Bioorg. Chem. 103 (2020) 104165.
[23] S. Wilt, et al., Further exploration of the structure-activity relationship of dual soluble epoxide hydrolase/fatty acid amide hydrolase inhibitors, Bioorg. Med. Chem. 51 (2021) 116507.
[24] J. Angelia, et al., Structure-activity relationship studies of benzothiazole-phenyl analogs as multi-target ligands to alleviate pain without affecting normal behavior, Prostag. Other Lipid Mediat. 164 (2023) 106702.
[25] E. Proschak, H. Stark, D. Merk, Polypharmacology by design: a medicinal chemist's Perspective on multitargeting compounds, J. Med. Chem. 62 (2) (2019) 420–444.
[26] G. Kumar, N.P. Singh, Synthesis, anti-inflammatory and analgesic evaluation of thiazole/oxazole substituted benzothiazole derivatives, Bioorg. Chem. 107 (2021) 104608.
[27] D.I. Ugwu, et al., Novel anti-inflammatory and analgesic agents: synthesis, molecular docking and in vivo studies, J. Enzym. Inhib. Med. Chem. 33 (1) (2018) 405–415.
[28] E.M.H. Abbas, et al., Synthesis, anti-inflammatory and antinociceptive activity of some novel benzothiazole derivatives, Res. Chem. Intermed. 41 (4) (2015) 2537–2555.
[29] S. Seth, A comprehensive Review on Recent advances in synthesis & Pharmacotherapeutic potential of benzothiazoles, Antiinflamm Antiallergy Agents Med Chem 14 (2) (2015) 98–112.
[30] P. Yadav, K. Shah, Quinolines, a perpetual, multipurpose scaffold in medicinal chemistry, Bioorg. Chem. 109 (2021) 104639.
[31] B. Jismy, et al., Efficient microwave-assisted Suzuki–Miyaura cross-coupling reaction of 3-bromo pyrazolo[1,5-a]pyrimidin-5(4H)-one: towards a new access to 3,5-diarylated 7-(trifluoromethyl)pyrazolo[1,5-a]pyrimidine derivatives, RSC Adv. 11 (3) (2021) 1287–1302.
[32] A.K. Sharma, et al., *Microwave-assisted Suzuki cross-coupling reaction, a key Step in the Synthesis of polycyclic aromatic Hydrocarbons and their metabolites.* The journal of organic chemistry 72 (23) (2007) 8987–8989.
[33] K. Ahn, et al., Discovery and characterization of a highly selective FAAH inhibitor that reduces inflammatory pain, Chem. Biol. 16 (4) (2009) 411–420.
[34] G.G. Muccioli, et al., Substituted 2-Thioxoimidazolidin-4-ones and imidazolidine-2,4-diones as fatty acid amide hydrolase inhibitors templates, J. Med. Chem. 49 (1) (2006) 417–425.
[35] X. Wang, et al., Synthesis and evaluation of benzothiazole-based analogues as novel, potent, and selective fatty acid amide hydrolase inhibitors, J. Med. Chem. 52 (1) (2009) 170–180.
[36] M. Mileni, et al., Crystal structure of fatty acid amide hydrolase bound to the carbamate inhibitor URB597: discovery of a deacylating water molecule and insight into enzyme inactivation, J. Mol. Biol. 400 (4) (2010) 743–754.
[37] C.A. Lipinski, Drug-like properties and the causes of poor solubility and poor permeability, J. Pharmacol. Toxicol. Methods 44 (1) (2000) 235–249.
[38] B.D. Hammock, et al., Movement to the clinic of soluble epoxide hydrolase inhibitor EC5026 as an analgesic for neuropathic pain and for use as a nonaddictive opioid alternative, J. Med. Chem. 64 (4) (2021) 1856–1872.
[39] D.F. Veber, et al., Molecular properties that influence the oral bioavailability of drug candidates, J. Med. Chem. 45 (12) (2002) 2615–2623.
[40] M. Gupta, et al., The blood-brain barrier (BBB) score, J. Med. Chem. 62 (21) (2019) 9824–9836.
[41] A. Garrido, et al., hERG toxicity assessment: Useful guidelines for drug design, Eur. J. Med. Chem. 195 (2020) 112290.
[42] A. Tjolsen, et al., The formalin test: an evaluation of the method, Pain 51 (1) (1992) 5–17.
[43] J. Angelia, et al., Structure-activity relationship studies of benzothiazole-phenyl analogs as multi-target ligands to alleviate pain without affecting normal behavior, Prostag. Other Lipid Mediat. 164 (2023) 106702.
[44] J.Y. Park, et al., Antinociceptive and anti-inflammatory Effects of recombinant Crotamine in mouse Models of pain, Toxins (10) (2021) 13 (Basel).
[45] H. Huang, et al., Development of highly sensitive fluorescent assays for fatty acid amide hydrolase, Anal. Biochem. 363 (1) (2007) 12–21.
[46] P.D. Jones, et al., Fluorescent substrates for soluble epoxide hydrolase and application to inhibition studies, Anal. Biochem. 343 (1) (2005) 66–75.
[47] R. Abagyan, M. Totrov, D. Kuznetsov, *ICM—a new method for protein modeling and design: Applications to docking and structure prediction from the distorted native conformation.* Journal of Computational Chemistry 15 (5) (1994) 488–506.